Exotic-atom measurement of the magnetic dipole moment of the Σ^- hyperon

D. W. Hertzog,* M. Eckhause, P. P. Guss,† D. Joyce, J. R. Kane, W. C. Phillips, W. F. Vulcan, R. E. Welsh, R. J. Whyley, and R. G. Winter
College of William and Mary, Williamsburg, Virginia 23185

E. Austin,‡ J. P. Miller, F. O'Brien,§ and B. L. Roberts
Boston University, Boston, Massachusetts 02215

G. W. Dodson**
Boston University, Boston, Massachusetts 02215
and Massachusetts Institute of Technology, Cambridge, Massachusetts 02139

R. J. Powers††
California Institute of Technology, Pasadena, California 91125

R. B. Sutton
Carnegie-Mellon University, Pittsburgh, Pennsylvania 15213

A. R. Kunselman
University of Wyoming, Laramie, Wyoming 82071
(Received 16 November 1987)

The magnetic dipole moment of the Σ^- hyperon has been determined from Σ^--atom x-ray transitions in natural lead and tungsten. Negative kaons were stopped in a target which consisted of sheets of W or Pb immersed in liquid hydrogen. The Σ^- resulting from the reaction $K^-p\rightarrow\Sigma^-\pi^+$ were tagged by observing the monoenergetic π^+. X rays from Σ^- atoms were detected by intrinsic Ge detectors. The x-ray lines were analyzed for fine-structure splitting and the magnetic moment was determined from the measured splitting. The value obtained for the magnetic moment is $\mu(\Sigma^-)=(-1.105\pm0.029\pm0.010)\mu_N$ where the first error is statistical and the second systematic. This value is in reasonable agreement with measurements that used precession techniques and with the theoretical predictions of simple quark models.

I. INTRODUCTION

Anomalous magnetic moments have played an important role in our understanding of subatomic structure. Whereas measurements of the g factors of the electron and muon have given no indication of lepton internal structure,[1] the large anomalous moments of the baryons support the picture of their composite structure. Their magnetic moments have served as important constraints on models of hadron structure. The first modern calculation of the baryon moments was carried out by Coleman and Glashow[2] shortly after the introduction of unitary symmetry by Gell-Mann[3] and Ne'eman.[4] The development of SU(6) and constituent-quark models[5,6] led to additional predictions. In the MIT bag model[7] light quarks are confined to a bag with a radius on the order of their Compton wavelength, so that the relativistic change of the confined particle's Dirac moment is included. Despite the development of QCD, calculations of the static properties of baryons have continued to evolve from a more phenomenological approach, since perturbative QCD breaks down at low energies.

In recent years baryon magnetic moments have continued to be the subject of much theoretical and experimental work. The magnetic dipole moments of the hyperons in the $J^P=\frac{1}{2}^+$ octet (except for the Σ^0) have been remeasured,[8–14] and the level of precision is now adequate to test detailed corrections to the simple models. The calculational approaches range from applying model-independent sum rules[15] to the inclusion of a pion field outside the bag to preserve chiral symmetry.[16,17]

The experiment which is reported here was performed in the C4 branch of the low-energy separated beam LESB I at the Brookhaven National Laboratory Alternating Gradient Synchrotron (AGS). A portion of these data was reported earlier,[11] and in this paper we present the analysis of all the data. A K^- beam of momentum 680 MeV/c was brought to rest in a laminar target which consisted of thin sheets of the target material immersed in a liquid-hydrogen (LH_2) bath (see Fig. 1). The reaction

$$K^-+p\rightarrow\Sigma^-+\pi^+ \text{ [branching ratio } (B)=460001] \quad (1)$$

was used to produce Σ^- hyperons. The monoenergetic $\pi^+(T_\pi=82.6$ MeV) which served to tag Σ^- production were detected using range scintillation spectrometers placed on both sides of the target. The $\Sigma^-(T_{\Sigma^-}=12.4$ MeV) were stopped in the target foils and formed exotic

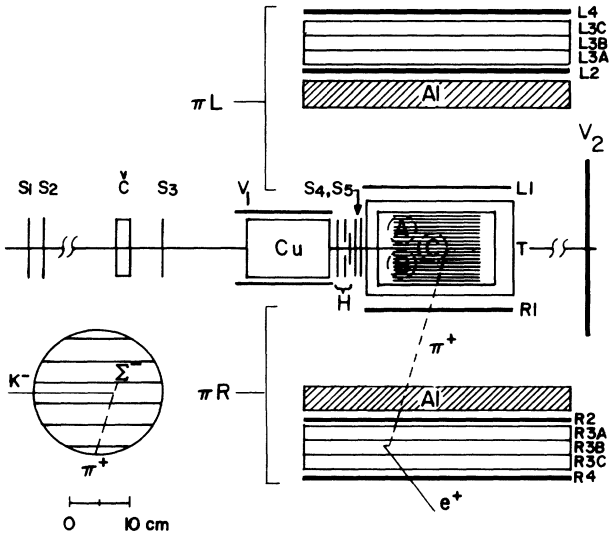

FIG. 1. Plan view of the experimental arrangement. S_1-S_5 are beam-defining scintillation counters; V_1 is a veto counter surrounding the Cu moderator; V_2, a downstream veto counter; H, a beam-defining hodoscope; πL and πR, pion spectrometers including Al moderator; and C, a Čerenkov counter to detect kaons. The laminar target assembly is shown with three Ge detectors located below. Inset: a typical $K^- p$ interaction in the LH_2 between the target sheets. (The inset is not to scale.)

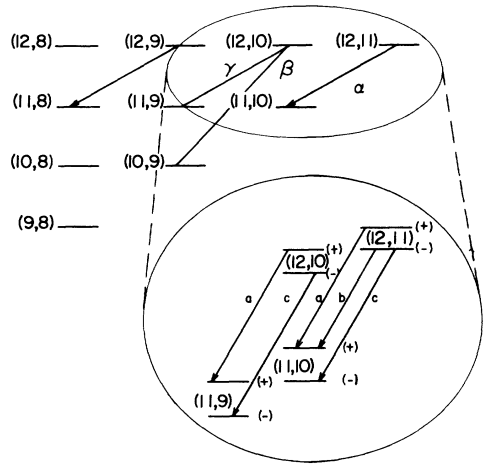

FIG. 2. A portion of the atomic cascade. The energy separations are not to scale.

atoms. X rays from these atoms were detected by three intrinsic reverse-electrode coaxial Ge detectors which were housed in a single upward-oriented cryostat.

The measured fine-structure splitting in the x-ray lines was used to determine the magnetic moment. The splitting $\delta E_{n,l}$ of an atomic level with principal quantum number n and orbital angular momentum l is approximately given by[18]

$$\delta E_{n,l}=(g_0+2g_1)(Z\alpha)^4\frac{m_\Sigma}{2n^3l(l+1)}\ , \tag{2}$$

where $g_0=-1$ is the Dirac moment and g_1 is the anomalous (Pauli) moment. The Σ^- magnetic moment is the sum of these two components, i.e.,

$$\mu(\Sigma^-)=(g_0+g_1)\frac{e}{2m_\Sigma}=(g_0+g_1)\left[\frac{m_p}{m_\Sigma}\right]\mu_N\ , \tag{3}$$

where μ_N is the nuclear magneton, and m_p and m_Σ are the proton and Σ masses, respectively ($\hbar=c=1$).

Figure 2 shows a portion of the atomic cascade. In the blow-up, adjacent fine-structure levels and the $E1$ transitions between them are given. Of the three $E1$ transitions, only a and c are of sufficient intensity to be observed experimentally, since the contribution from the spin-flip ($\Delta j=0$) transition b is negligible for large principal quantum numbers.

Experimentally one observes a doublet whose components are separated in energy by

$$\Delta E=\delta E_{n_f l_f}-\delta E_{n_i,l_i}\ , \tag{4}$$

where n_i,l_i and n_f,l_f are the quantum numbers of the upper and lower atomic states, respectively. A measurement of ΔE is used to determine the magnetic moment.

II. EXPERIMENTAL DETAILS

At a transport momentum of 680 MeV/c, the C4 beam at the AGS had a $\pi^-:K^-$ ratio of $\sim$9:1 and an incident K^- flux of $\sim$60 000 with 4×10^{12} protons incident per burst on a Pt production target. An incident beam particle was identified with scintillation counters (labeled $S_1\cdots S_5$ in Fig. 1). The particles were slowed down in a Cu moderator, and their position as they entered the target was determined by a hodoscope (labeled H in Fig. 1). Once the nominal degrader thickness was determined from a range curve, it was adjusted to maximize the yield of the kaonic ($n=9\rightarrow n=8$) transition. The Cu degrader was surrounded by a plastic veto counter V_1 which eliminated events in which a secondary particle scattered out of the side of the degrader. This veto reduced the trigger rate by about 10%.

Beam pions were rejected by a velocity-selective Čerenkov counter $\check{C}$ and by measurements of dE/dx in counter S_5. The Čerenkov counter consisted of a Lucite radiator viewed by six RCA8850 photomultiplier tubes. At the transport momentum of 680 MeV/c, π^- Čerenkov light is totally internally reflected. The efficiency of the Čerenkov counter was checked using time of flight. When coincidences between four or more of the six tubes were required, $\check{C}$ was found to have an efficiency of 94% for detecting kaons. The pion rejection factor was 49:1.

A diagnostic dE/dx spectrum from S_5 is shown in Fig. 3 for which the trigger included the Čerenkov requirement. During data collection the discriminator threshold on S_5 was raised to further suppress pion related events. The signature for a stopping kaon was $K_{\rm stop}=S_1\cdot S_2\cdot\check{C}\cdot S_3\cdot S_4\cdot S_{5(\rm high)}\cdot\bar{V}_1\cdot\bar{V}_2$ where V_2 was a veto counter placed downstream of the target.

The target consisted of 19 metal foils of the target ele-

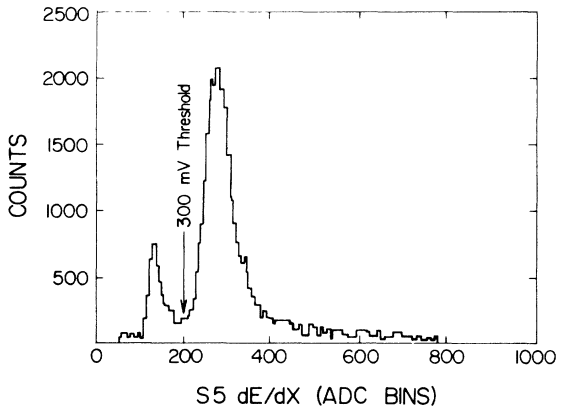

FIG. 3. dE/dx spectrum from S_5. The Čerenkov counter is in the trigger. The peak above the 300-mV threshold is from slow K^-. The smaller peak to the left of the K^- peak is from π^- which fire the Čerenkov counter.

ment placed parallel to the beam and immersed in liquid hydrogen. The foils were spaced 0.46 cm apart, and were 15.0 cm in length. They were placed in a cylindrical vessel such that the center sheet was 10.5 cm high and the outermost sheet 6.5 cm. The Pb foils were 0.035 cm thick and the W foils were 0.023 cm thick, which in both cases gives a thickness of 0.4 g/cm^2. The optimal foil thickness and spacing were determined from Monte Carlo calculations. Factors important in the design were (a) the LH_2-to-foil mass ratio to optimize kaon stops in the hydrogen, (b) foil spacing so that loss of Σ^- from decay was minimized, and (c) foil thickness adequate to stop Σ^- but thin enough to minimize absorption of the subsequent x rays in the plates.

The x-ray spectroscopy system was designed to detect photons in the energy range of 100 to 700 keV with good resolution and efficiency. Energy resolution was the most important consideration since the separation of the doublet components is less than 0.2% of the transition energy. The detector assembly was placed so that the top faces of the crystals were 12 cm below the beam center. The resolution [full width at half maximum (FWHM)] of these detectors under beam conditions was in the range of 900 to 1100 eV in the energy interval of the Σ^- x rays of interest, with an absolute photopeak efficiency of $\sim 20\%$. The detectors were equipped with special pulse processors which rejected events separated by less than 45 μsec. This feature reduced pile-up problems to a minimum, but limited the beam rate at which data could be collected to $\sim 14\,000$ K^- stops per AGS slow extracted beam spill.

The instrumental response to monoenergetic photons from radioactive sources was studied before and after the running period, and was monitored continuously during the running period. The calibration sources were chosen so that the γ-ray energies spanned the region of interest, but did not coincide with K^- or Σ^- x rays. In addition to ^{137}Cs and ^{57}Co sources, which were always present, ^{133}Ba was used in conjunction with the Pb target, and ^{192}Ir was used with the W target. The energies of the calibration lines were taken from the compilation by Lorentz.[19]

The π^+ range spectrometers used to tag Σ^- production were essential components in this experiment. The monoenergetic π^+ from the reaction given in Eq. (1) emerged from the target cryostat with an energy between 60 and 82 MeV, depending on the number of foils traversed. With the target foils placed as described above, Monte Carlo calculations showed that π^+ which emerged within a cone of 30° from the sides of the target were the optimal tag for Σ^- most likely to stop in the target foils. The counters in the range telescope labeled $3A-3C$ in Fig. 1 were $45.7\times45.7\times2.54$ cm^3 Ne 102 plastic scintillators. These were sandwiched between counters 0.635 cm thick, the front one serving as an entrance counter and the back serving as a veto. The thickness of the aluminum degrader was adjusted to optimize the number of π^+ stopping in the spectrometer. The effective fractional solid angle of each range telescope was ~ 0.09 when counter $3A$ was positioned 36 cm from the beam line center.

To discriminate against π^- from the reaction

$$K^- + p \rightarrow \Sigma^+ + \pi^- \quad (B = 20\%) ,$$

it was necessary to observe the $\pi^+ \rightarrow \mu^+ \rightarrow e^+$ decay chain. Since the μ^+ has a mean life of 2.2 μsec, an 8-μsec gate was chosen to observe the decay positron. If a second beam particle was incident on the target during this period, the gate was blanked off for 40 nsec so that scattered or secondary particles did not mimic a decay positron. A typical timing spectrum for the decay positrons is shown in Fig. 4. A fit to these data for the muon lifetime gave 2.26 ± 0.10 μsec, in agreement with the accepted value.[20]

The data-acquisition system consisted of a PDP 11/34 interfaced to CAMAC through a Bi-Ra microprogrammable branch driver (MBD). Each event initiated by a K^- stop signature in coincidence with a count in one of the x-ray detectors was sorted as either a *tagged* or an *untagged* event. *Tagged* events were those accom-

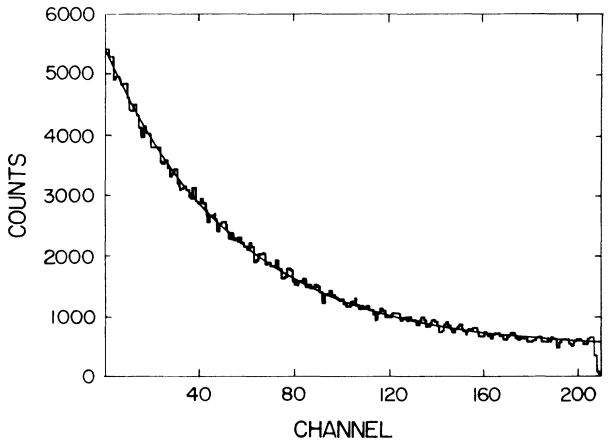

FIG. 4. Pion range spectrometer timing spectrum of delayed e^+ signatures following K^- stops. The data were fitted to the function $Ae^{-t/\tau}+B$. The value obtained for τ from this sample of data was 2.26 ± 0.10 μsec, characteristic of the $\pi^+ \rightarrow \mu^+ \rightarrow e^+$ decay chain.

panied by a π^+ signature in one of the range telescopes, and all others were sorted as *untagged* events. For each event the following information was written to magnetic tape: a header, the energy deposited in the Ge detector, Ge detector time relative to a K^- stop, the hodoscope pattern, dE/dx information for S_4 and S_5, and kaon time of flight. For *tagged* events the following additional information was written: which counters in the range spectrometer fired from the (delayed) e^+, the e^+ energy deposited in the range spectrometer and the time between a K^- stop and the decay positron.

Events in which the Ge detectors fired in coincidence with a 1.0-μsec gate opened by (AGS on)$\cdot S_1\cdot S_2\cdot S_3\cdot S_4\cdot S_5\cdot \bar{V}_1$ were also recorded. These events, which included random coincidences between the gate initiated by a beam pion and a γ ray from one of the radioactive sources, were recorded as beam-on calibration events. During the beam-off portion of the AGS spill cycle, ungated histograms covering the regions of the ^{57}Co 122.06-keV and the ^{137}Cs 661.66-keV γ rays were accumulated in the MBD. Every 10 min these histograms were written to tape and then cleared. These histograms were fitted on-line to provide a monitor of the gain of the x-ray spectrometer system and off-line they provided a two-point stabilization correction for each 10-min interval of data. Additional calibration sources were studied several times when the AGS was not running to check the relative efficiency and linearity of the detector–amplifier–analog-to-digital-convertor (ADC) systems.

Monte Carlo studies, carried out before this experiment was performed, showed that if a background γ ray were to lie under an x-ray peak, it would present serious problems for the magnetic moment determination if the intensity of the γ line were greater than 10% of the Σ^- x-ray intensity. To search for such γ rays in the energy regions of interest, negative pions were stopped in targets of Pb, W, and U. These background studies were carried out in a preliminary run in the test channel of the Los Alamos Meson Physics Facility. In addition, at the end of the Brookhaven running period, a 220-MeV/c π^- beam from LESB I was stopped in the Pb and U targets. In a subsequent study, the W target was placed in a low-energy pion beam from the muon channel at the AGS. No evidence was found in the Pb or W data for contaminants in the regions of the Σ^- x rays used for the magnetic-moment measurement. There was evidence that a contaminant line fell under the $\Sigma^-(12\rightarrow 11)$ transition in uranium.

III. ANALYSIS CONSIDERATIONS

A. Atomic physics

The relative intensities $a:b:c$ of the transitions shown in Fig. 2 can be calculated[18] for a statistical population of the states. If one defines $\Delta n=-1$ circular transitions as those between levels with $l=n-1$ and noncircular transitions as those between levels with $l\leq n-2$, the intensities are given by

$$\text{circular: } a:b:c=(2n^2+n-1):1:(2n^2-n-1) \tag{5a}$$

and

$$\text{first noncircular}(l=n-2):\quad a:b:c=(2n^2-3n):1:(2n^2-5n+2)\ , \tag{5b}$$

where n is the principal quantum number of the lower state.

The Dirac equation, with vacuum-polarization potentials as given by Blomqvist,[21] was integrated by the method of Borie[22] to obtain the energies of the Σ^- atomic levels. Perturbation techniques use the expression for fine-structure splitting given in Eq. (2) corrected for radiative and relativistic effects, while in Borie's method, the recoil effects discussed by Pilkuhn[23] are automatically included. Screening of the Coulomb field by the atomic electrons was calculated using the parametrization of Vogel.[24] Nuclear polarization was included separately following Ericson and Hüfner.[25] Borie[26] estimates that the vacuum-polarization and recoil corrections can be calculated reliably to better than 0.5 eV. Since our result depends on energy differences between levels rather than on absolute energies, the sensitivity to systematic errors in the calculated energy levels is reduced. The overall accuracy of the calculated transition energies should be better than ± 1 eV.

In Fig. 5 we show the fine structure for the $n=10$, $l=9$, and $n=10$, $l=8$ Σ^- levels in Pb. First we show the Dirac levels, then the Dirac levels corrected for vacuum polarization, recoil, finite nuclear size and nuclear polarization, and finally the inclusion of the anomalous moment term, where the value of g_1 was taken to be -0.42 [$\mu(\Sigma^-)=-1.11\mu_N$; see Eq. (3)]. For a negative magnetic moment the atomic states of higher j lie higher in energy. From Eq. (2) it is clear that for some positive value of g_1, one could also obtain the same fine-structure splitting, but the higher-j state would then lie lower in energy.

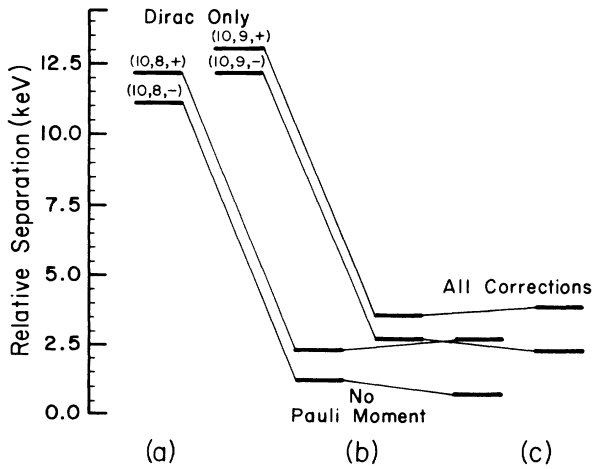

FIG. 5. Relative positions of the energy levels of the Pb Σ^- ($n=10$, $l=9$) and ($n=10$, $l=8$) states. The states are labeled with the quantum numbers n,l, and + if $j=l+\frac{1}{2}$ and − if $j=l-\frac{1}{2}$. 5(a) shows the Dirac levels, 5(b) shows the inclusion of all other corrections except the anomalous moment, and 5(c) shows the fully corrected levels assuming $\mu(\Sigma^-)=-1.11\mu_N$.

In the analysis it was necessary to include the presence of noncircular transitions in addition to the corresponding circular transitions. In the case shown in Fig. 2, the circular transition is labeled α and the first noncircular is labeled γ. From Fig. 5 one can see that for any value of the magnetic moment, the relative separations between all the levels are fixed, and therefore the energy differences between the four observed lines (a and c) shown in Fig. 2 are fixed. Thus the presence of noncircular transitions does not add additional free parameters to the analysis. Once the value of the magnetic moment is fixed for a particular fit, the energy separation between all the transitions and the intensities within a doublet are determined by the atomic physics. The resulting complex line shape is thus well understood. The only uncertainty is the intensity of the noncircular doublet relative to the circular one. As discussed below, this intensity was determined from a cascade calculation which was constrained to reproduce the measured yields of the Σ^- x rays. The uncertainty in this contribution was included in the systematic error.

It has been pointed out that the g factor of a bound particle is decreased relative to its free value.[27] This effect has been demonstrated[28] to be considerable for a μ^- bound in the $1s$ level of a high-Z muonic atom. In our experiment, where the lowest principal quantum state considered is the $n=10$ state, this effect was estimated to be smaller than 0.1% and was neglected in our analysis.

B. Cascade calculations and experimental x-ray yields

Since the transitions labeled α and γ were not experimentally resolved in energy, it was necessary to simulate the atomic cascade in order to determine the relative intensities of noncircular to circular transitions. To compare the experimental with the calculated x-ray yields, it was necessary to determine the detector efficiency and the absorption of x rays in the target foils as a function of energy. The dependence of the detector efficiency on energy was studied with γ lines of well-known relative intensity from radioactive sources. The absorption of x rays in the target foils was studied both experimentally with sources and by Monte Carlo calculations.

The relative efficiency for each detector was determined by comparing the observed intensities of γ rays from ^{133}Ba, ^{75}Se, ^{192}Ir, and ^{154}Eu with their tabulated intensities.[19] These calibration data were taken in the laboratory with the same data acquisition hardware and software used in the x-ray experiment. The area under each photopeak was determined by integrating a large region containing the peak, and then subtracting an interpolated background which was determined by integrating a region on either side of the peak. The results from the different sources were normalized to the 356.0-keV line of ^{133}Ba. The normalized data and a polynomial fit of the form log(relative efficiency) versus energy are shown in Fig. 6 for detector B. The data for the other detectors were similar.

A duplicate Pb target was used to measure x-ray absorption in the target sheets. With the outer shell and insulation removed, the target assembly was placed above

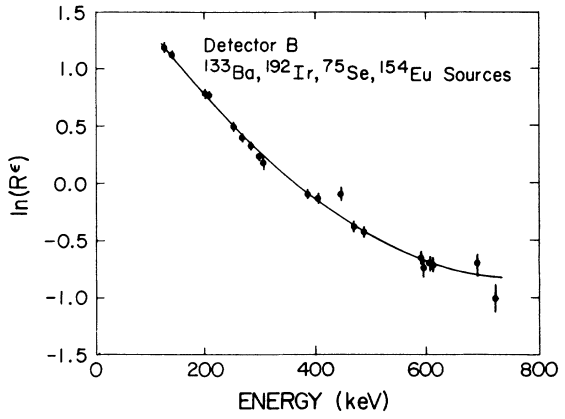

FIG. 6. Detector relative efficiency as a function of x-ray energy for one of the detectors. The solid curve represents a polynomial fit to the data.

the detector in the geometry of the experiment. Radioactive sources sandwiched between Pb foils half the thickness of the target foils were placed sequentially at each of 24 points on a three-dimensional lattice within the target. Spectra were collected at each point for a time period proportional to the kaon stopping density calculated with a Monte Carlo program. The relative efficiency measurements were done as before, and the measured (transmission$\times$efficiency), $\epsilon_{\rm lab}(E)$, is shown along with a fifth-order polynomial fit in Fig. 7. Also shown in the figure is the result of a Monte Carlo program which used the distribution of stopping kaons to calculate the distribution of Σ^- stops in the target sheets. From this distribution, the transmission$\times$efficiency function, $\epsilon_{\rm MC}(E)$, was calculated from the tabulated photon cross sections[29] and measured detector efficiency (Fig. 6).

Below 300 keV, the two methods diverge, presumably because in this low-energy range more than half of the

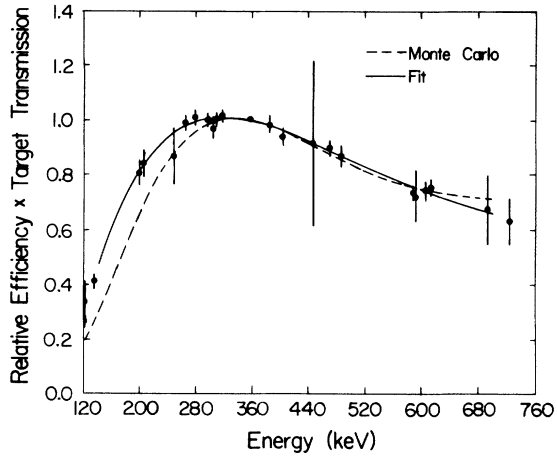

FIG. 7. The transmission efficiency product for the Pb target and one of the detectors as a function of x-ray energy. The dashed curve is the result of a Monte Carlo calculation; the solid curve represents a polynomial fit to the data.

photons are absorbed and the transmission×efficiency product is more sensitive to the assumptions used in the calculation.

The average of the measured and Monte Carlo transmission×efficiency factor was used in the analysis of the lead data. A systematic error of

$$\frac{|\epsilon_{\text{lab}}(E)-\epsilon_{\text{MC}}(E)|}{2}$$

was included in the analysis for yields. Since a duplicate target was not available for W, the Monte Carlo results were used for it. The same systematic error as determined for Pb was included in the analysis of the W data.

The intensities of both the kaonic and Σ^- x-ray lines were determined by fitting each transition to a single Gaussian plus background with all parameters free. The area was determined from[30]

$$\text{area} = \text{amplitude}\times\text{FWHM}\times 1.06 .$$

This area was then corrected for target absorption and detector efficiency to determine the relative yield. The kaonic x-ray intensities were compared with those of Wiegand and Godfrey[31] and found to be in good agreement, with a χ^2 per degree of freedom of 8.6/9.

To determine the intensity of the noncircular transitions, calculations simulating the Σ^- atomic cascade were performed using a code developed by Leon and Seki.[32] This calculation was constrained to reproduce the measured yields of the Σ^- x-ray transitions. The Σ^- were distributed in an initial state of principal quantum number $n=25$. Electric dipole radiative and Auger transitions as well as nuclear absorption of the hadrons from the atomic levels were included in the calculation. Transitions with $\Delta n=-2$, such as the one labeled β in Fig. 2, were experimentally resolved in energy from the $\Delta n=-1$ transitions. The yields of the $\Delta n=-2$ transitions are quite sensitive to the input parameters in the cascade calculation as discussed below.

Nuclear absorption of the Σ^- was included in the calculation using an optical potential of the form[33]

$$v=-\frac{2\pi}{m}\left[1+\frac{m_\Sigma}{m_n}\right]\bar{a}\rho(r) ,$$

where m is the Σ-nucleus system reduced mass and $\rho(r)$ is the nuclear matter distribution which was assumed to be equal to the charge density determined from electron scattering. Initially the value of the strong-interaction scattering length $\bar{a}$ was taken to be that determined[33] from low-Z Σ^- atoms, $\bar{a}=(0.35+i0.20)$ fm. It was found that the calculated yield of the x rays was not sensitive to the real part of $\bar{a}$; however, a value of 0.30 fm for the imaginary part resulted in a better fit to the data.

An additional parameter which was varied to improve the agreement between calculated and experimental yields was the l distribution of hadrons in the initial atomic level $n_{\max}$. Rather than a statistical population of $(2l+1)$ for each l state in the levels $(n_{\max},l)$ a population of $(2l+1)e^{\zeta l}$ was assumed.[32] The best-fit value of the distribution parameter ζ was 0.28 for Pb and 0.097 for W. The experimental and calculated yields for the Σ atomic x rays are given in Table I. The uncertainty in the fraction f_{nc} of noncircular transition present was determined by fitting the measured yields to the calculated ones, and then changing the cascade calculation input parameters ζ and $\bar{a}$ unitl χ^2 increased by one unit. The calculated intensities of the noncircular transitions are given in Table II.

IV. DATA ANALYSIS

A portion of the data was analyzed to study the influence of various cuts on the x-ray signal-to-background ratio. This ratio was improved in the untagged spectra by using the information from the beam hodoscope. No software cuts were found which improved this ratio in the tagged data without a severe loss in good events. Separate untagged and tagged histograms for each detector were formed with a gain shifting program which assumed two-point stabilization as mentioned above. The beam-on calibration spectra were subjected to the same gain-shifting procedure as the x-ray data. These calibration spectra were then used to determine the resolution and gain for each detector-amplifier-ADC system.

Although it was expected that the approximation of a Gaussian detector response should be adequate, extensive studies of the sensitivity of the extracted value of the magnetic moment to assumed detector line shapes were carried out to test this hypothesis. A detector response which included the effects of small-angle Compton scattering in the target, charge trapping in the crystal

TABLE I. Relative intensities of Σ^- Pb and Σ^- W transitions.

Pb transition	Experimental relative intensity	Cascade calculation	W transition	Experimental relative intensity	Cascade calculation
15→14	0.82±0.23	0.83			
14→13	0.92±0.17	0.91	14→13	0.94±0.14	0.85
13→12	0.95±0.08	0.96	13→12	0.91±0.14	0.94
12→11	1.00	1.00	12→11	1.00	1.00
11→10	1.101±0.03	0.97	11→10	0.94±0.07	1.02
10→9+13→11	0.58±0.05	0.59	10→9+13→11	0.84±0.07	1.00
15→13	0.091±0.018	0.084	14→12	0.13±0.02	0.13
14→12	0.079±0.017	0.078	12→10	0.13±0.02	0.10

TABLE II. Calculated relative intensities of the noncircular (nc) to circular transitions with the circular amplitude equal to 1.0. The uncertainties on the last two digits are given in parentheses.

Target	Transition	First nc
Pb	$\Sigma(12\rightarrow 11)$	0.121(24)
	$\Sigma(11\rightarrow 10)$	0.022(05)
W	$\Sigma(11\rightarrow 10)$	0.120(20)

and pulse pileup in the amplifier[34] was used to analyze a portion of the data. When the same set of data was analyzed for fine-structure splitting using a simple Gaussian function, no statistically significant difference in the value of the extracted moment was obtained.

The data were divided into subsets representing time periods over which the resolutions of the three detectors remained constant. Three blocks for Pb (Pb1, Pb2, Pb3), and two for W (W1, W2), were necessary. The resolutions for each detector are listed for the different blocks in Table III. The energies listed correspond to the Σ^- x-ray transition energies of interest.

In Figs. 8 and 9 we show samples of the untagged and tagged spectra from natural tungsten. As expected, the untagged spectrum contains prominent kaonic x-ray lines and rather low-intensity Σ^- x rays, while the reverse is true in the tagged spectra. The signal-to-background ratio for the Σ^- x rays in the untagged spectra is $\sim 60\%$ better than that observed in the earlier Σ^- atom experiments.[35,36] This improvement is due both to better detector resolution and to enhanced Σ^- production from the liquid hydrogen. The tagging technique resulted in an improvement of 15 in the Σ^- x-ray signal-to-background ratio over the earlier experiments[35,36] in which K^- were stopped in a target sheet of natural Pb.

The Σ^- x-ray lines in both the untagged and tagged spectra were analyzed for fine-structure splitting. It was assumed that the complex, unresolved line in the spectrum consisted of two circular transitions and two less intense noncircular transitions. Noncircular transitions with $l < n-2$ were neglected since the cascade calculations predicted relative intensities of less than 1% for these transitions. A function of the form

$$F(x;n,l,g_1)=D_c(x;n,l,g_1)+f_{nc}D_{nc}(x;n,l,g_1)+B(x) \tag{6}$$

was used to describe the complex x-ray line shape. Both functions labeled $D(x;n,l,g_1)$ are doublets which describe the two transitions a,c shown in Fig. 2. The subscripts c and nc refer to circular or noncircular transitions, respectively, and f_{nc} is the fraction of noncircular transition present. The term $B(x)$ represents the background under the peak. A second-order polynomial adequately represented the backgrounds encountered in both the calibration and data spectra.

Each doublet function consisted of two Gaussian functions of the form

$$D_c(x;n,l,g_1)=A\exp\left[-\left[\frac{x-x_0}{\sqrt{2}\sigma}\right]^2\right]+R_cA\exp\left[-\left[\frac{x-[x_0+\Delta(g_1)]}{\sqrt{2}\sigma}\right]^2\right] \tag{7a}$$

and

$$D_{nc}(x;n,l,g_1)=A\exp\left[-\left[\frac{x-[x_0+\epsilon(g_1)]}{\sqrt{2}\sigma}\right]^2\right]+R_{nc}A\exp\left[-\left[\frac{x-[x_0+\epsilon(g_1)+\Delta'(g_1)]}{\sqrt{2}\sigma}\right]^2\right], \tag{7b}$$

where n,l are the principal and orbital angular momentum quantum numbers of the lower atomic state and Δ (Δ') is the separation of the two circular (noncircular) components labeled a and c in Fig. 2 [see Eq. (4)]. The quantity $\epsilon(g_1)$ is the separation between corresponding spin-up ($j=l+\frac{1}{2}$) to spin-up circular and noncircular transitions and is determined if the value of the anomalous moment g_1 is fixed. Furthermore, the energy

TABLE III. Detector resolution (in eV) at the energies of the $\Sigma(12\rightarrow 11)$ and $\Sigma(11\rightarrow 10)$ transitions in Pb and the $\Sigma(11\rightarrow 10)$ transition in W whose nominal energies are 283, 373, and 303 keV, respectively. The uncertainties on the last two digits are given in parentheses. The three detectors are indicated by the suffixes *A*, *B*, and *C* and the numbers 1, 2, and 3 indicate different blocks of running time. The doublet separations of these three transitions are 371, 655, and 431 eV, respectively, for $\mu(\Sigma^-)=-1.158\mu_N$.

Group	FWHM (at 283 keV)	FWHM (at 373 keV)	Group	FWHM (at 303 keV)
Pb1(*A*)	910.4(1.0)	1011.4(1.0)	W1(*A*)	979.2(1.0)
(*B*)	934.9(3.5)	1041.2(2.3)	(*B*)	989.0(5.8)
(*C*)	969.6(3.6)	1093.4(2.2)	(*C*)	1058.8(5.4)
Pb2(*A*)	927.5(5.4)	1029.2(3.2)	W2(*A*)	979.2(1.0)
(*B*)	950.8(7.5)	1058.2(4.5)	(*B*)	989.0(5.8)
(*C*)	979.9(6.4)	1102.1(3.6)	(*C*)	1058.8(5.4)
Pb3(*A*)	929.8(4.1)	1043.1(2.5)		
(*B*)	965.7(2.5)	1065.1(1.4)		
(*C*)	1002.3(10.2)	1127.9(5.9)		

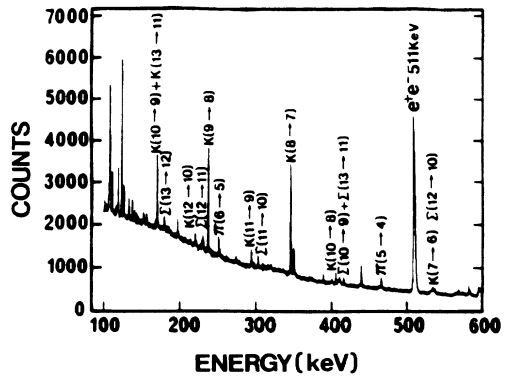

FIG. 8. One set of untagged W x-ray data. Intense K^- x rays and weaker (secondary) Σ^- and π^- x rays are visible.

differences Δ, Δ', and ϵ are functions of n and l as well as of g_1. The intensity ratios R_c and R_{nc} were determined from Eqs. (5a) and (5b). The detector resolution σ was obtained from the calibration spectra. The only free parameters in the fit were the amplitude A, the centroid x_0, and the background parameters. All other quantities in Eq. (6) except f_{nc} could be calculated uniquely for a given value of g_1. The noncircular intensity f_{nc} was obtained from the cascade calculation described above.

To analyze each composite x-ray peak for fine-structure splitting, a series of least-square fits to the functional form given in Eq. (6) was performed. The value of the anomalous moment g_1 was held fixed for each fit, but was incremented in steps corresponding to $0.01\mu_\Sigma$ between fits so that χ^2 could be mapped out as a function of Δ and thus of g_1. In principle this procedure should be sensitive to the sign of the moment since the two doublet components have different intensities. However, for small values of the anomalous moment the sensitivity of this experiment to the sign vanishes. Monte Carlo studies showed that with the detector resolution available to this experiment, there is little sensitivity to the sign for a magnitude of $\mu(\Sigma^-)$ less than $1.2\mu_N$.

A χ^2 map from a sample of the $\Sigma^-(11\rightarrow 10)$ transition in W is shown in Fig. 10(a). Two equally probable values corresponding to a negative or positive magnetic moment

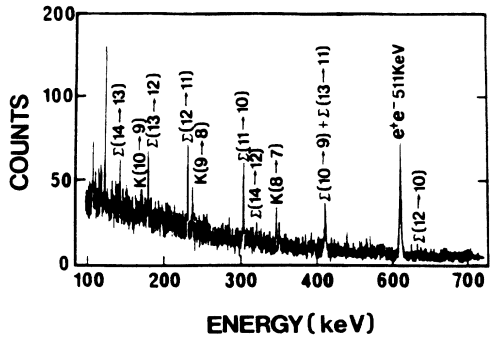

FIG. 9. The equivalent tagged W x-ray data. The Σ^- x rays are enhanced by the tagging technique.

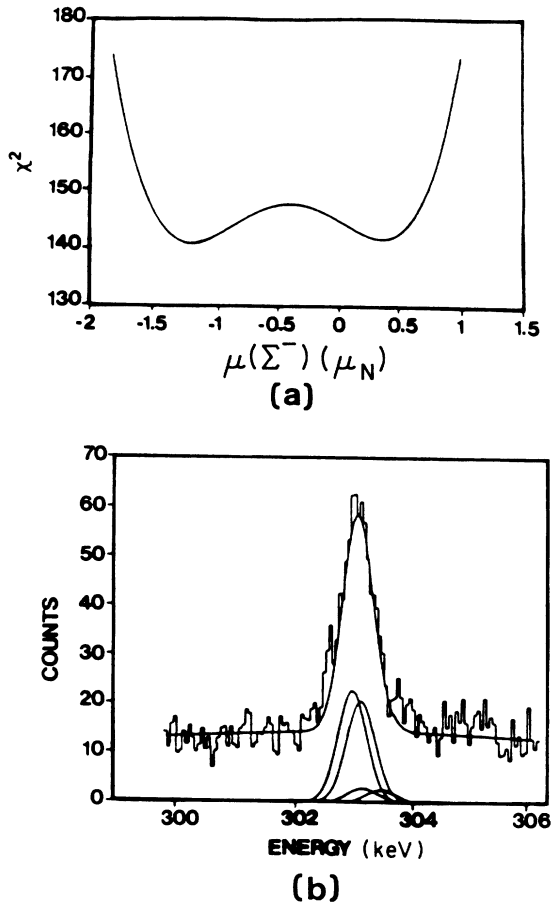

FIG. 10. (a) A sample χ^2 map from the analysis of the $\Sigma(11\rightarrow 10)$ transition in W. There were 116 degrees of freedom. The magnetic moment $\mu(\Sigma^-)$ is given in units of μ_N. (b) The best fit to the subset of W data used to generate the χ^2 map in (a) with the magnetic moment set to the value at the χ^2 minimum. The circular and noncircular doublet components are shown separately.

are permitted. The value of $\mu(\Sigma^-)$ corresponding to zero-energy separation between the fine-structure components (the local maximum) is at least 3 standard deviations away from the most probable value of the moment. This sample represents about 7% of the data, and when the χ^2 maps from the three detectors and all the transitions and targets are added together this becomes greater than a 10-standard-deviation effect. In Fig. 10(b) we show the best fit to the $\Sigma^-(11\rightarrow 10)$ transition in W. The value obtained for $\mu(\Sigma^-)$ for this fit was $-1.14\mu_N$. The individual doublet components are shown in Fig. 10(b).

The validity of this method of extracting peak separations which are of the order of half a linewidth was checked in several ways. Functions described by Eq. (6) were generated with background amplitudes and signal amplitudes comparable to those expected in the experiment. The number of counts in each channel of the calculated function was then distributed about the calculated value with Gaussian statistics. Several of these "data

sets" were generated with different random number seeds. It was found that for input negative magnetic moments as small in magnitude as $0.5\mu_N$ it was still possible to obtain the input value, within statistics, from the analysis routines.

An additional check was made with γ-ray lines from radioactive sources with energy differences comparable to the expected separations. Spectra from ^{203}Hg, ^{75}Se, and ^{182}Ta were collected separately. The 279.197-keV line from ^{203}Hg, the 264.651- and 279.528-keV lines from ^{75}Se, and the 264.075-keV line from ^{182}Ta were fit to Gaussian functions to determine the amplitudes and FWHM for each peak. A background spectrum was collected using Compton-scattered photons from ^{60}Co. The spectra from ^{203}Hg and ^{75}Se were summed with the background to form a doublet at $\sim$279 keV with components separated by 331 eV. A second doublet was formed from the ^{75}Se and ^{182}Ta spectra at $\sim$264 keV with a doublet separation of 576 eV. In both cases the analysis routines gave the correct separation to within the statistical errors.

Lastly, the data sets were checked for self-consistency by dividing them into smaller portions to look for systematic problems over the weeks of data collection. In all cases the data were found to be self-consistent.

V. RESULTS

The systematic errors encountered in the analysis of the tagged data were studied in detail. The influence of uncertainties in the instrumental resolution and in the fraction of the noncircular transition was studied by changing these parameters over a range of values.

The values of f_{nc} used are given in Table II. The sensitivity of the value of the magnetic moment to the amount of noncircular transition was determined by changing the noncircular contribution, f_{nc} in Eq. (6), by $\pm 1\sigma$ from the cascade prediction described above. In only one case was this an important effect. For the Pb $\Sigma^-(12\rightarrow 11)$ transition this effect represented a $\pm 0.016\mu_N$ uncertainty. For the other two transitions included in this analysis this contribution to the systematic error was less than $\pm 0.01\mu_N$.

Since the $n=10$, $l=9$ levels of Σ^- Pb and W are expected to have strong-interaction widths of a few eV, it was necessary to include this effect in the analysis for fine-structure splitting. The $(n=10, l=9)$ level widths calculated with the optical potential discussed above are 23 ± 7 and 4 ± 2 eV for Pb and W, respectively. The strong-interaction width of the W $\Sigma^-(10,9)$ level was negligible and was not included in the analysis. An extra 12 eV was added[37] to the instrumental widths given in Table III for the analysis of the Pb $\Sigma^-(11\rightarrow 10)$ transition. With this additional width the value of $\mu(\Sigma^-)$ obtained from the Pb $\Sigma^-(11\rightarrow 10)$ transition changes by $0.01\mu_N$, well within the statistical precision of the measurement. These lower levels will also have strong-interaction shifts on the order 0.1 of the widths. We have assumed that both fine-structure components of each lower level are shifted by the same amount.

The sensitivity of the value obtained for the moment to the region over which the data were fit was checked and only for the Pb $\Sigma^-(12\rightarrow 11)$ transition was there any statistically significant change. This was attributed to the close proximity of both the $K^-(9\rightarrow 8)$ x ray and a nuclear γ ray. For this transition the largest change in $\mu(\Sigma^-)$ that resulted from fitting over a wide range of regions was included as an error.

To obtain the magnetic moment, the χ^2 maps from the tagged data for each of the three detectors from the several transitions were summed together. The $\Sigma^-(12\rightarrow 11)$ and $\Sigma^-(11\rightarrow 10)$ transitions in Pb and the $\Sigma^-(11\rightarrow 10)$ transition in W were used to determine the magnetic moment. The summed χ^2 map is shown in Fig. 11. The negative sign is preferred only at the 1σ level. However, only the negative value is consistent with the recent precession experiments.[10,13,14] The value obtained from the summed χ^2 map for all the tagged data is

$$\mu(\Sigma^-)=(-1.105\pm 0.029\pm 0.010)\mu_N\ ,$$

where the first error is statistical and the second is systematic.

To demonstrate the self-consistency of the data represented in Fig. 11 we plot in Fig. 12 the individual magnetic moment values obtained from each summed set of tagged data by detector and transition. The solid line through the data is the value quoted above and the dashed lines are $\pm 1\sigma$ (statistical only). The χ^2/ν is 0.97. The result quoted above is derived from 24 independent measurements obtained from two Σ^- atomic transitions in Pb and one in W, and the use of three separate x-ray detectors.

We have also analyzed the untagged data from the Pb and W targets. Analysis of the Pb $\Sigma^-(11\rightarrow 10)$ and W $\Sigma^-(11\rightarrow 10)$ transitions in the untagged data gave $\mu(\Sigma^-)=(-1.090\pm 0.031)\mu_N$, consistent with the tagged results. However, the Pb $\Sigma^-(12\rightarrow 11)$ transition, gave a value of $\mu(\Sigma^-)=(-1.394\pm 0.051)\mu_N$ which is 5σ from the result obtained in the analysis of the tagged data. To search for nuclear γ rays which might lie under the Pb $\Sigma^-(12\rightarrow 11)$ transition, we have examined the energy re-

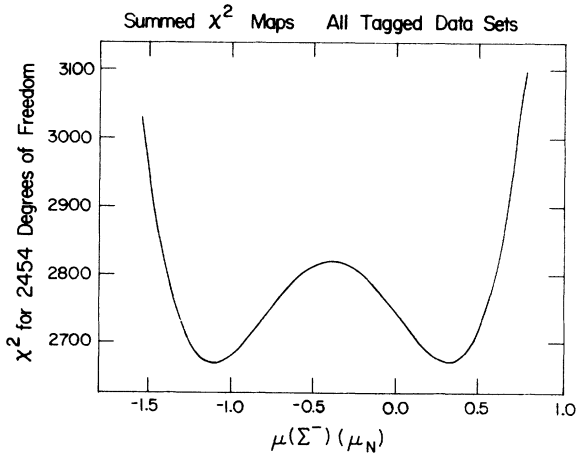

FIG. 11. The final χ^2 map for all tagged data. The minimum is at $-1.105\mu_N$ for which the χ^2/ν is 1.09.

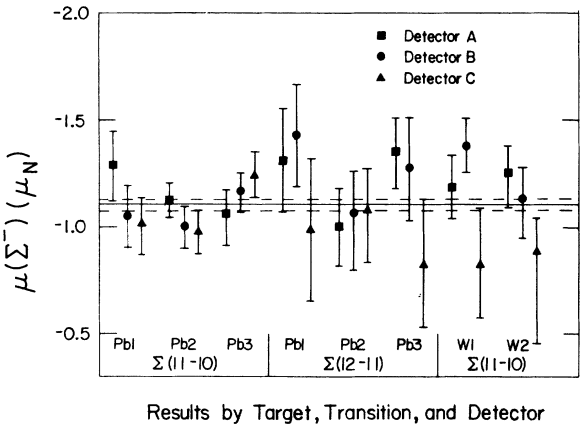

FIG. 12. Magnetic moment values obtained for each subgroup of data. Results from each transition and detector are shown separately.

gion around 283 keV in spectra produced by stopping π^- in Pb, as well as in the beam-on calibration spectra (in-flight π^-). We found no significant contaminant γ lines. Although we do not understand the source of this discrepancy, we must assume that a contaminant γ-ray line exists in the untagged data, but is sufficiently suppressed by the tagging technique so that the tagged result is not sensitive to this complication.

Since the result obtained from the untagged Pb $\Sigma^-(12\rightarrow 11)$ transition agrees with the first measurements of the Σ^- magnetic moment[35,36] determined from data equivalent to the untagged Pb data of this experiment, we disregarded these early measurements, which were almost exclusively from the $\Sigma^-(12\rightarrow 11)$ transition in Pb, when taking a "world average."

A depleted uranium target, in addition to the Pb and W targets reported on above, was also used in the present experiment. In the earlier experiment by this group[38] and also in the experiment by the Columbia-Yale Collaboration[39] a contaminant γ ray appeared to coincide with the U $\Sigma^-(12\rightarrow 11)$ x ray. Although such a contaminant was not seen in the tagged or untagged U spectra obtained in this experiment, the value extracted for the magnetic moment was substantially larger than that obtained from any other tagged transition. To search for possible contaminant γ rays, π^- were stopped in the uranium target. Although no clear contaminant line appeared at 358 keV, the U $\Sigma^-(12\rightarrow 11)$ transition energy, a possible candidate for producing such a γ ray is ^{154}Eu (a fission fragment). Unambiguous identification of other fission fragments[40] was obtained in the γ-ray spectra from stopping π^-, K^-, and Σ^-. Since a companion transition to the nuclear ground state has the same energy as the $K_{\beta 2}$ electronic x ray in U, the positive identification of this line was not straightforward. However, by examining ratios of the $K_{\beta 1}$, $K_{\beta 2'}$, and $K_{\beta 3}$ electronic x rays in the three spectra, it was possible to construct a strong circumstantial case for the presence of this companion transition in the untagged and tagged spectra from stopping K^- in U.

VI. DISCUSSION AND CONCLUSIONS

Several measurements of the Σ^- magnetic dipole moment have recently been made. Despite the small Σ^- decay asymmetry parameter[20] of -0.068 ± 0.013, the polarizations and high energies available at Fermilab have permitted precession measurements to be carried out. The first precession result[10] for $\mu(\Sigma^-)$ was $(-0.89+0.14)\mu_N$, in fair agreement with the result obtained in this experiment.

Wah *et al.*[13] obtained the result $\mu(\Sigma^-)=(-1.23\pm0.03\pm0.03)\mu_N$, which does not agree well with the current measurement. Recently that collaboration has reported a value of $\mu(\Sigma^-)=(-1.166\pm 0.014\pm0.010)\mu_N$ from a new measurement[14] using precession data from both Σ^- β decay (where the decay asymmetry is almost 100%) and the $n\pi^-$ hadronic weak decay.

Precision measurements of the magnetic dipole moments of all the baryons in the $\frac{1}{2}^+$ octet, except for the Σ^0, are now available. In Table IV we show the current experimental values of the moments, along with several

TABLE IV. Experimental and theoretical magnetic moments of the baryons in the $J^P=\frac{1}{2}^+$ octet in units of μ_N. Experimental values are from Ref. 20 except where indicated otherwise.

Baryon	Experiment	De Rújula *et al.* (Ref. 5)	SU(6)[a]	MIT bag (Ref. 7)	Cloudy bag (Ref. 17)	Isgur-Karl (Ref. 6)	Relativistic quarks (Ref. 43)
p	2.793	2.79	2.69	input	2.60	2.85	2.60
n	−1.913	−1.86	−1.99	−1.862	−2.01	−1.85	−1.55
Λ	−0.613±0.004	−0.60	−0.64	−0.712	−0.58	−0.61	−0.61
Σ^+	2.379±0.020	2.67	2.44	2.71	2.34	2.54	2.42
Σ^-	−1.158±0.022[b]	−1.05	−1.05	−1.01	−1.08	−1.00	−0.99
Ξ^0	−1.250±0.014	−1.39	−1.32	−1.56	−1.27	−1.20	−1.25
Ξ^-	−0.69 ±0.04	−0.46	−0.52	−0.64	−0.51	−0.43	−0.60

[a]Broken SU(6) with pionic corrections (Ref. 42).

[b]Average of this work, Refs. 10, 13, and 14. The magnetic moment values reported in Ref. 14 from Σ^- β decay and from the $n\pi^-$ hadronic weak decay were treated as independent measurements. The combined error was scaled up by a factor of 1.496 as suggested by the Particle Data Group (Ref. 20).

calculations. The value of the Σ^- moment represents the average of this experiment and those of Refs. 10, 13, and 14. Earlier exotic atom measurements are omitted for the reasons discussed above.

Fair agreement exists between the calculations and measurements, but only at the 10–20 % level. A number of attempts have been made recently to improve the simple constituent-quark model. The model-independent analyses of Franklin[15] and Lipkin[41] show that nonstatic contributions may be important, a point also emphasized by Isgur and Karl.[6] Pionic contributions have been studied in the context of the bag model[16,17] and as a correction to the usual static model.[42] Relativistic wave functions have also been considered[43] and the predictions for values of the hyperon moments are in agreement with the measured values, although the neutron and proton moments obtained in this calculation are not very satisfactory. The experimental precision now available is sufficient to provide detailed tests of the models of baryon structure, but the present theoretical attempts to describe these data fall short of a complete understanding.

ACKNOWLEDGMENTS

We wish to acknowledge the important efforts of R. Pehl, F. Goulding, D. Landis, and N. Madden of the Lawrence Berkeley Laboratory, and R. Trammell of EG&G Ortec in developing the Ge detectors and associated electronics. We thank the AGS staff and BNL hydrogen target group for their continued support of this experiment. We also wish to thank the Los Alamos Meson Physics Facility for the use of the LAMPF test beam and N.J. Colella, K.L. Giovanetti, R.D. Hart, C. Kenney, J. Kraiman, J. Ginkel, and D. R. Tieger for their help on parts of the experiment. We thank E. Borie, M. Blecher, M. Leon, and R. Seki for use of their computer codes. We wish to thank P. Cooper, E. McCliment, and R. Winston for providing us with results before publication, and for helpful discussions on the Fermilab experiments. Several of us wish to thank S.L. Glashow and K. Johnson for interesting discussions on magnetic moments and baryon structure. This work was supported in part by the U.S. National Science Foundation and the Department of Energy.

---

*Present address: Department of Physics, University of Illinois, Urbana, IL 61801.

†Present address: EG&G Energy Measurements, Box 380, Suitland, MD 20746.

‡Present address: MIT Lincoln Laboratories, Box 73, Lexington, MA 02173.

§Present address: AT&T Bell Laboratories, Whippany, NJ 07981.

**Present adddress: MIT Laboratory for Nuclear Science, Cambridge, MA 02139.

††Present address: Institut für Physik der Universität Basel, CH-Basel 4056, Switzerland.

[1]V. W. Hughes and T. Kinoshita, Commun. Nucl. Part. Phys. **14**, 341 (1985).

[2]S. Coleman and S. L. Glashow, Phys. Rev. Lett. **6**, 423 (1961).

[3]M. Gell-Mann, Caltech Report No. CTSL-20, 1961 (unpublished).

[4]Y. Ne'eman, Nucl. Phys. **26**, 222 (1961).

[5]A. De Rújula, H. Georgi, and S. L. Glashow, Phys. Rev. D **12**, 147 (1975).

[6]N. Isgur and G. Karl, Phys. Rev. D **21**, 3175 (1980).

[7]T. DeGrand, R. L. Jaffe, K. Johnson, and J. Kiskis, Phys. Rev. D **12**, 2060 (1975).

[8]P. T. Cox *et al.*, Phys. Rev. Lett. **46**, 877 (1981).

[9]C. Ankenbrandt *et al.* Phys. Rev. Lett. **51**, 863 (1983).

[10]L. Deck *et al.* Phys. Rev. D **28**, 1 (1983).

[11]D. W. Hertzog *et al.*, Phys. Rev. Lett. **51**, 1131 (1983).

[12]R. Rameika *et al.*, Phys. Rev. Lett. **52**, 581 (1984).

[13]Y. W. Wah *et al.*, Phys. Rev. Lett. **55**, 2551 (1985).

[14]G. Zapalac *et al.*, Phys. Rev. Lett. **57**, 1526 (1986).

[15]J. Franklin, Phys. Rev. D **29**, 2648 (1984), and references therein.

[16]G. E. Brown, M. Rho, and V. Vento, Phys. Lett. **84B**, 383 (1979).

[17]S. Théberge and A. W. Thomas, Nucl. Phys. **A393**, 252 (1983), and references therein.

[18]H. A. Bethe and E. Salpeter, *Quantum Mechanics of One- and Two-Electron Atoms* (Academic, New York, 1957).

[19]A. Lorentz, *Nuclear Decay Data for Radionuclides used as Calibration Standards* [IAEA Nuclear Data Section Report No. INDC(NDS)-145/GEI, 1983].

[20]Particle Data Group, M. Aguilar-Benitez *et al.*, Phys. Lett. **170B**, 1 (1986).

[21]J. Blomqvist, Nucl. Phys. **B48**, 95 (1972).

[22]E. Borie, Phys. Rev. A **28**, 555 (1983), and references therein.

[23]H. Pilkuhn and H. G. Schlaile, Phys. Rev. A **27**, 657 (1983), and references therein.

[24]P. Vogel, At. Data Nucl. Data Tables **14**, 599 (1974); P. Vogel *et al.*, Phys. Lett. **70B**, 39 (1977), and references therein.

[25]T. E. O. Ericson and J. Hüfner, Phys. Lett. **40B**, 459 (1972).

[26]E. Borie (private communication).

[27]H. Margenau, Phys. Rev. **57**, 383 (1940); K. W. Ford, V. W. Hughes, and J. G. Wills, *ibid.* **129**, 194 (1963).

[28]T. Yamazaki *et al.*, Phys. Lett. **53B**, 117 (1974).

[29]E. Storm and H. I. Israel, At. Nucl. Data Tables **7**, 565 (1970).

[30]P. R. Bevington, *Data Reduction and Error Analysis for the Physical Sciences* (McGraw-Hill, New York, 1969), p. 248.

[31]C. E. Wiegand and G. L. Godfrey, Phys. Rev. A **9**, 2282 (1974).

[32]M. Leon and R. Seki, Phys. Rev. Lett. **32**, 132 (1974).

[33]C. J. Batty, Nucl. Phys. **A372**, 433 (1981).

[34]W. Phillips (unpublished).

[35]B. L. Roberts *et al.*, Phys. Rev. D **12**, 1232 (1975).

[36]G. Dugan *et al.*, Nucl. Phys. **A254**, 396 (1975).

[37]D. H. Wilkinson, Nucl. Instrum. Methods **95**, 259 (1971).

[38]J. D. Fox *et al.*, Phys. Rev. Lett. **31**, 1084 (1973).

[39]G. Dugan (private communication).

[40]D. P. Russell III, Senor Distinction thesis, Boston University, 1985 (unpublished).

[41]H. J. Lipkin, Phys. Rev. D **24**, 1437 (1981); Nucl. Phys. **B214**, 136 (1983).

[42]J. Franklin, Phys. Rev. D **30**, 1542 (1984).

[43]Z. Dziembowski and L. Mankiewicz, Phys. Rev. Lett. **55**, 1839 (1985).